

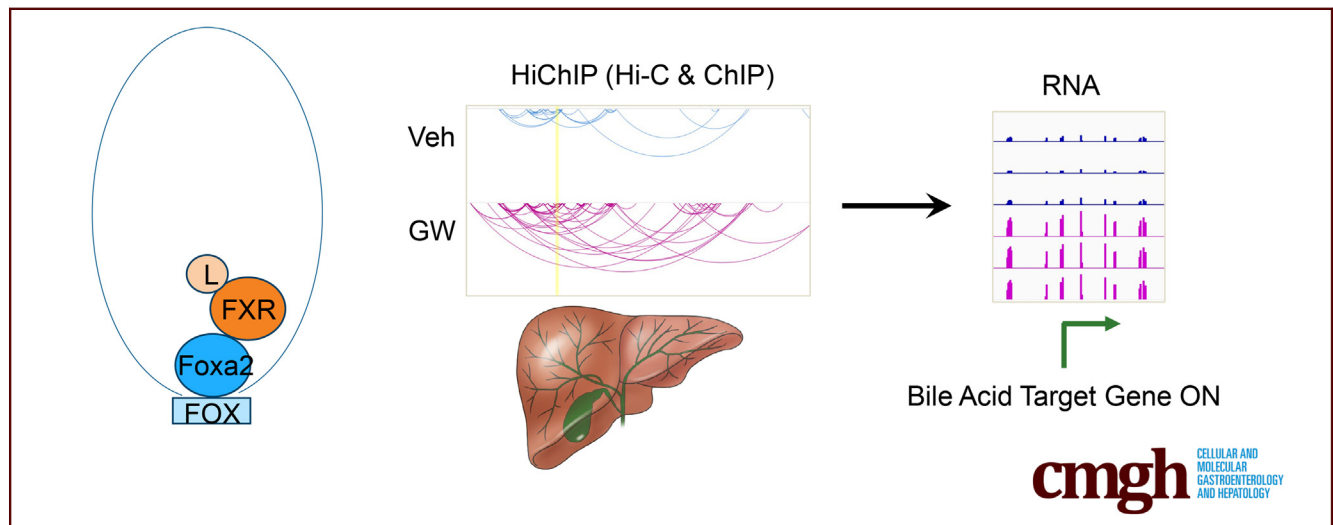
ORIGINAL RESEARCH

Pioneer Factor Foxa2 Mediates Chromatin Conformation Changes for Activation of Bile Acid Targets of FXR



Yi Hao, Lu Han, Anqi Wu, and Irina M. Bochkis

Department of Pharmacology, University of Virginia, Charlottesville, Virginia



SUMMARY

Ligand-dependent activation of bile acid receptor FXR is associated with enormous changes in chromatin architecture, including increase in global interactions and redistribution of topological associated domains. These changes are mediated by pioneer factor Foxa2.

BACKGROUND & AIMS: Transcription factors regulate gene expression that orchestrates liver physiology. Many bind at distal enhancers and chromatin looping is required to activate their targets. Chromatin architecture has been linked to essential functions of the liver, including metabolism and sexually dimorphic gene expression. We have previously shown that pioneer factor Foxa2 opens chromatin for binding of nuclear receptors farnesoid X receptor (FXR) and liver X receptor- α during acute ligand activation. FXR is activated by bile acids and deletion of Foxa2 in the liver results in intrahepatic cholestasis. We hypothesized that Foxa2 also enables chromatin conformational changes during ligand activation and performed genome-wide studies to test this hypothesis.

METHODS: We performed Foxa2 HiChIP (Hi-C and ChIP) to assess Foxa2-dependent long-range interactions in mouse livers treated with either vehicle control or FXR agonist GW4064.

RESULTS: HiChIP contact analysis shows that global chromatin interactions are dramatically increased during FXR activation.

Ligand-treated livers exhibit extensive redistribution of topological associated domains and substantial increase in Foxa2-anchored loops, suggesting Foxa2 is involved in dynamic chromatin conformational changes. We demonstrate that chromatin conformation, including genome-wide interactions, topological associated domains, and intrachromosomal and interchromosomal Foxa2-anchored loops, drastically changes on addition of FXR agonist. Additional Foxa2 binding in ligand-activated state leads to formation of Foxa2-anchored loops, leading to distal interactions and activation of gene expression of FXR targets.

CONCLUSIONS: Ligand activation of FXR, and likely of related receptors, requires global changes in chromatin architecture. We determine a novel role for Foxa2 in enabling these conformational changes, extending its function in bile acid metabolism. (*Cell Mol Gastroenterol Hepatol* 2024;17:237–249; <https://doi.org/10.1016/j.jcmgh.2023.10.009>)

Keywords: Transcriptional Regulation; Bile Acid Metabolism; Foxa2; Nuclear Receptors.

Transcription factors regulate gene expression that orchestrates liver physiology.^{1,2} Many bind at distal enhancers^{3,4} and chromatin looping between these enhancers and proximal promoters is required to activate their targets. Recent reports link chromatin architecture to essential hepatic functions, including metabolism⁵ and sexually dimorphic gene expression,⁶ and dysregulation at

the chromatin level can lead to liver disease.^{5,7} Hence, it is critical to understand how 3-dimensional genome organization establishes hepatic transcription.

Activation of nuclear receptors, a family of ligand-dependent transcription factors, is used extensively in pharmacology to develop drug targets for diverse medical conditions, including metabolic disease and cancer.^{8–11} Farnesoid X receptors (FXR), liver X receptors (LXR), and peroxisome proliferator-activated receptors, members of the nuclear receptor family, are essential for metabolic homeostasis, regulating targets in bile acid, cholesterol, fatty acid, and glucose metabolism.¹² A previous model regarding ligand activation of these receptors involved a ligand-independent binding mechanism, depending on corepressor/coactivator exchange leading to activation of gene expression with addition of the ligand. However, we have shown that FXR and LXR α exhibit both ligand-independent and ligand-dependent binding, with chromatin accessibility being induced during ligand activation allowing for additional binding. These changes and activation of ligand-responsive gene expression require pioneer factor Foxa2.¹³

We have characterized a comprehensive role for winged-helix transcription factor Foxa2 in hepatic bile acid metabolism. Deletion of Foxa2 in the liver leads to intrahepatic cholestasis, and expression of FOXA2 is markedly decreased in liver samples from individuals with different cholestatic syndromes.¹ In addition, bile acid-dependent activation of nuclear receptor FXR to induce gene expression to protect liver from injury requires Foxa2.¹⁴ Furthermore, we demonstrated that that bile acid-induced inflammation in young Foxa2 mutants, once chronic, affected global metabolic homeostasis as they aged, leading to age-onset obesity.¹⁵

In this study, we hypothesized that Foxa2 enables chromatin conformational changes during ligand activation of FXR. We performed Foxa2 HiChIP to assess Foxa2-dependent long-range interactions in mouse livers treated with either vehicle control or FXR agonist GW4064. HiChIP contact analysis shows that global chromatin interactions are substantially increased during FXR activation. We demonstrate that chromatin conformation, including genome-wide interactions, topological associating domains (TADs), and intrachromosomal and interchromosomal loops, drastically changes on addition of FXR ligand. Hence, we determine a novel role for Foxa2 in enabling these conformational changes, extending its function in bile acid metabolism.

Results

Global Chromatin Interactions Are Increased During FXR Activation


We demonstrated previously that Foxa2 plays an extensive role in bile acid metabolism^{1,14,15} and is required for ligand-dependent activation of FXR.¹³ To test the hypothesis that, in addition to opening chromatin, Foxa2 is involved in chromatin conformation changes to enable ligand-dependent activation of FXR, we performed Foxa2 HiChIP (Hi-C and ChIP, study design in Figure 1) in mice treated with either vehicle control or FXR ligand GW4064 acutely (4 hours). The rationale was to assess chromatin

conformation changes before substantial physiological effects. HiChIP paired-end reads were mapped and filtered for valid interactions using HiC-Pro.¹⁶ Hi-C maps of all valid interactions show more chromatin loops in ligand-activated condition than in vehicle control (Figure 2A). Next, genome wide intrachromosomal bin pairs were filtered for an interaction distance between 20 kb and 2 Mb to identify statistically significant interactions. Representative arc-plots of significant chromatin interactions in both conditions on chromosome X are shown in Figure 2B, with more observed in ligand-activated livers. Number of total significant interactions increases with addition of FXR agonist (14,778 total interactions specifically for vehicle, 27,357 specifically for GW4064, 93,480 common for both, bin size 50 kb, false discovery rate [FDR] <0.001; Figure 2C). Scanning motif analysis of positional weight matrices in the JASPAR and TRANSFAC databases in genomic regions associated with significant interactions identified highly enriched forkhead motif bound by Fox transcription factors in both conditions (*P* value \sim 0), as expected for Foxa2 ChIP. Then, we performed differential significant contact analysis between 2 conditions (statistics per chromosome in Figure 3A, 31,891 total). An example of a genomic region (chr11:17600000–17800000) with increased chromatin interactions in ligand-treated condition is shown in Figure 2D. A virtual 4C plot shows increased signal in GW-treated livers and the difference (Δ) between 2 conditions (Figure 2E). To identify functional differences in differential interactions we mapped these regions to closest genes using GREAT¹⁷ and performed ingenuity pathway analysis (IPA). Overrepresented pathways included “Oxidative Stress,” “Fatty Acid Metabolism,” and “Acute Phase Response” for genes in interaction regions in control livers, whereas genes in FXR and CAR activation pathways and those regulating cholesterol metabolism were found in genes in interaction regions in agonist-treated livers, consistent with bile acid activation (Figure 3B). IPA of genes in differential interaction regions identified multiple upstream regulators, including HNF4 α , CEBPB, and EP300 for control livers and NFE2L2, SMARCB1, and chenodeoxycholic acid (Figure 3C) and chenodeoxycholic acid-regulated network (Figure 3D) for GW-treated livers. Chenodeoxycholic acid is a naturally occurring bile acid that activates FXR. Hence, IPA analysis confirms FXR activation in agonist-treated livers.

FXR Agonist Treatment Significantly Changes TAD Distribution

We proceeded to call TAD in our HiChIP data and found a comparable number in vehicle and GW-treated conditions

Abbreviations used in this paper: ChIP, chromatin immunoprecipitation; FDR, false discovery rate; FXR, farnesoid X receptor; HiChIP, combination of Hi-C and ChIP; IPA, ingenuity pathway analysis; LXR, liver X receptor; TAD, topological associated domain.

 Most current article

© 2023 The Authors. Published by Elsevier Inc. on behalf of the AGA Institute. This is an open access article under the CC BY-NC-ND license (<http://creativecommons.org/licenses/by-nc-nd/4.0/>).

2352-345X

<https://doi.org/10.1016/j.jcmgh.2023.10.009>

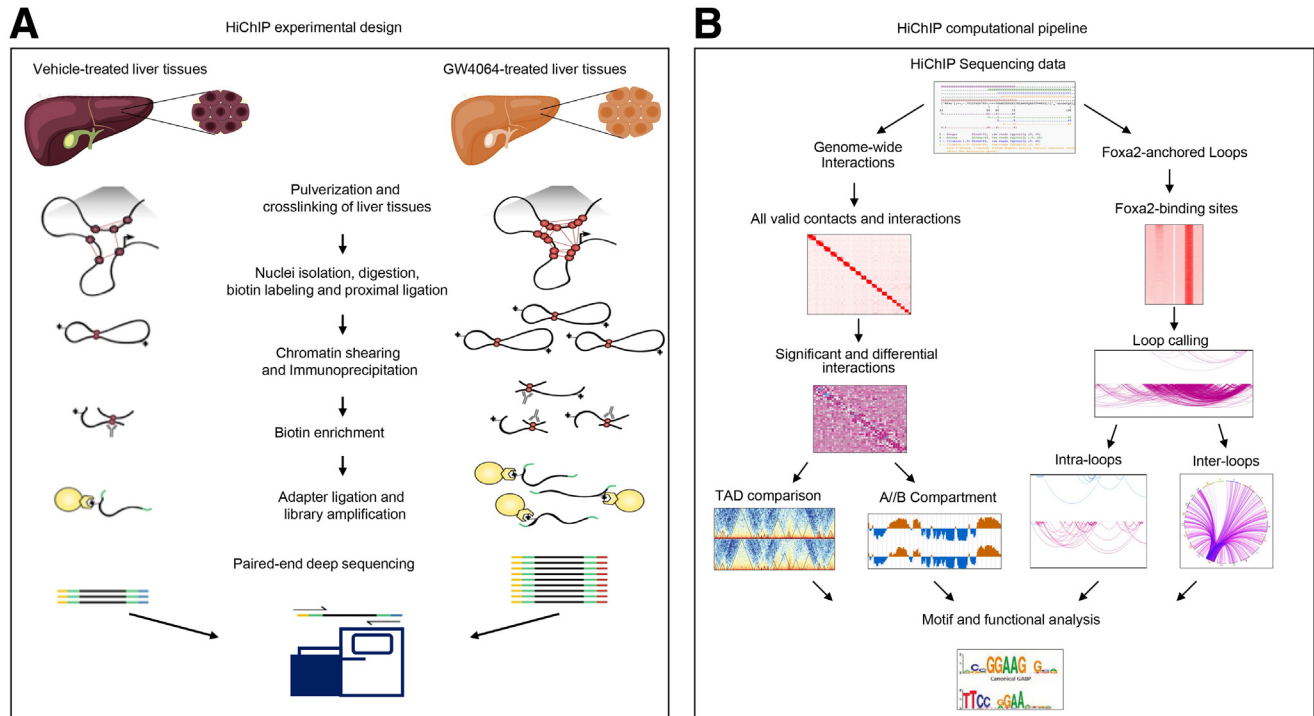


Figure 1. Study design and computational analysis pipeline. (A) HiChIP experimental design. Liver tissues were pulverized and crosslinked. Nuclei were isolated, nuclear membranes were permeabilized, chromosomes were digested with both MboI and HinfI, and the ends of DNA fragments were biotin-labeled. The proximal ends were ligated. Then, crosslinked chromatin was sheared into fragments. Foxa2 antibody was added and Foxa2-bound chromatin was immunoprecipitated. The HiChIP DNA fragments were enriched for biotin and were ligated with adapters. The HiChIP libraries were amplified by polymerase chain reaction and sent for paired-end deep sequencing. (B) HiChIP computational pipeline. First, we identified genome-wide valid interactions, significant interactions, and differential interactions in vehicle control and GW4064-treated livers. We proceeded to call TADs and compartments (activated Compartment A and repressed Compartment B) from genome-wide valid interaction data. In parallel, we used peaks from Foxa2 ChIP-Seq¹³ that also have signal in HiChIP data to identify Foxa2-anchored chromatin loops, divided into intrachromosomal and interchromosomal. We performed scanning motif analysis of sequences in these regions and mapped them to genes, which were used subsequently for functional analysis.

(3575 for vehicle, 3734 for GW4064). However, only a third of the TADs overlapped, whereas most TADs differed (1295 overlapping TADs, 2436 differential TADs; Figure 4A). Distribution of differential TADs on each chromosome is shown in Figure 5A. Next, we identified activated and repressed regions (Compartment A and Compartment B, respectively) in HiChIP interactions and found that 54 such regions changed from being activated in vehicle-treated to repressed in GW-treated livers, whereas 152 moved from Compartment A in agonist-treated to Compartment B in control livers (Figure 4B). Examples of full and partial switching are shown in Figure 4C and D.

For functional analysis, we mapped differential TADs to closest genes using GREAT¹⁷ and selected 1000 genes that mapped closest to the transcription start site for pathway analysis with Enrichr.²⁰ Overrepresented pathways included “LXR regulation of gluconeogenesis” and “FXR and LXR regulation of cholesterol metabolism,” consistent with bile acid activation, and “Cohesin loading onto chromatin,” congruous with cohesin function in mediating chromatin loop formation (Figure 5B, top).²¹ We also used published ChIP-Seq data sets in the mouse genome and intersected differential TAD regions and the binding data present in the

ChEA database, identifying overlap with RUNX1, TP53, β -catenin, and LXR targets (Figure 5B, bottom, ChEA analysis in Enrich). RUNX1 improves bile-acid induced hepatic inflammation in cholestasis,²² p53 plays a role in bile acid metabolism by regulating SHP (*Nr0b2*),²³ and β -catenin regulates FXR-dependent gene expression in cholestasis.²⁴ Hence our analysis of differential TADs identified regulators important for bile acid homeostasis and shows that ligand-dependent activation of FXR is associated with substantial changes in TAD distribution.

Functional analysis of genes in compartment-switched regions shows “Cytoskeletal Organization,” “Reactive Oxygen Species,” and “RXR/VDR pathway” pathways overrepresented in 54 regions repressed with agonist treatment and “Proteins with Altered Expression in Aging,” “Sodium/Proton Exchangers,” and “Opening of Calcium Channels” in 152 regions activated with GW treatment (Figure 5C).

Foxa2-Anchored Loops Are Drastically Increased Genome-Wide and at Bile Acid Targets

To relate Foxa2 binding sites to changes in chromatin conformation, we used previously called bound regions in

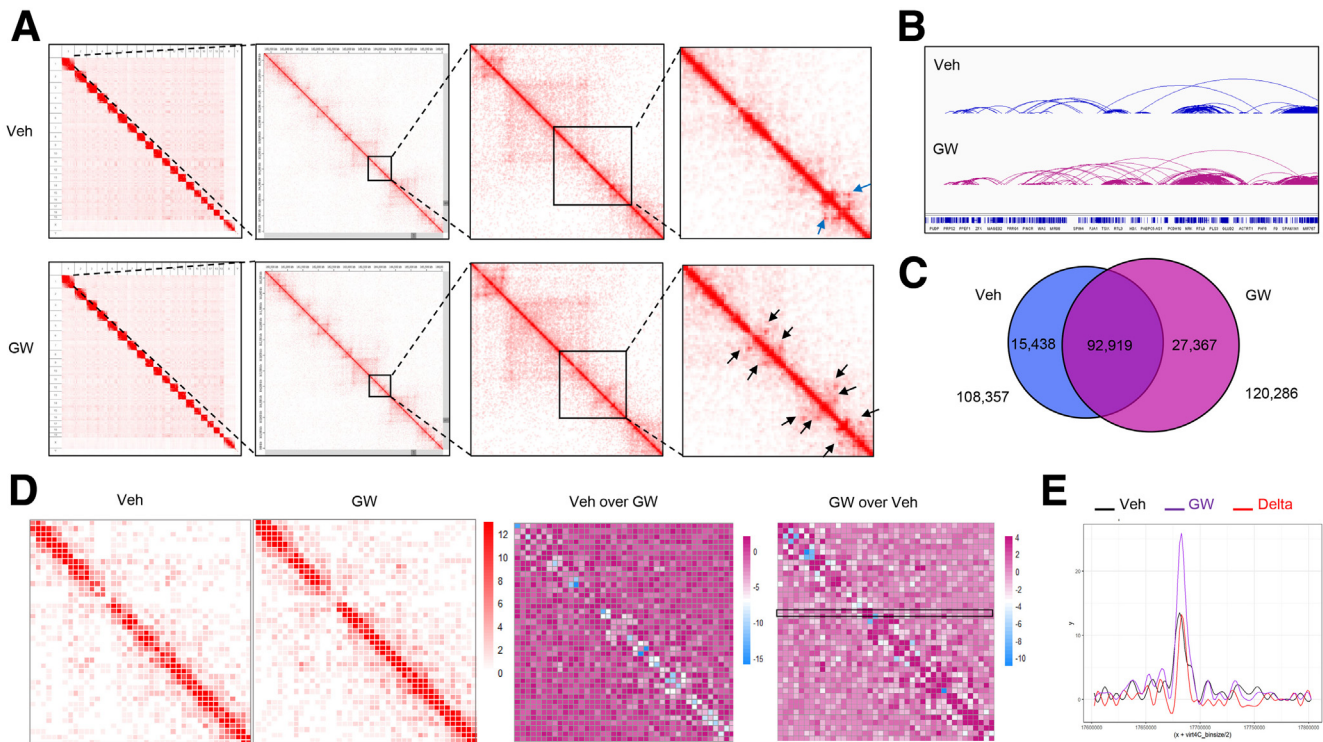


Figure 2. Genome-wide chromatin interactions increase during ligand-dependent activation of FXR. (A) Hi-C maps of all valid interactions in vehicle and GW4064-treated livers visualized with Juicebox¹⁸ at increasing zoom scales from left to right. Red squares along the diagonal in the left-most panel (top for vehicle, bottom for GW4064) represent the interactions within each chromosome territory. In the middle 2 panels (top for vehicle, bottom for GW4064), TADs are shown in plaid pattern along the diagonal. In the right-most panel (top for vehicle, bottom for GW4064), the arrows indicate presence of “corner peaks” of chromatin interactions at the edges of TADs, revealing the presence of chromatin loops. The blue arrows indicate interaction loops unique to vehicle treatment, whereas the black arrows specify those specific to GW4064 treatment, showing more chromatin loops with addition of agonist. (B) Integrative Genome Viewer (IGV)¹⁹ view of representative arc-plots of significant chromatin interactions in vehicle- and GW-treated conditions on chromosome X. (C) Venn diagram showing that the numbers of significant chromatin interactions increased with the addition of FXR agonist (14,778 total interactions specifically for vehicle, 27,357 specifically for GW4064, 93,480 common for both, under bin size of 50 kb and with the FDR values <0.001). (D) Comparison of differential interactions within a specific genomic region (chr11: 17600000–17800000), showing increased chromatin interactions with GW4064 treatment compared with vehicle in this region. Two left-most panels display the Hi-C maps along the diagonal within this genomic region for vehicle and GW4064 treatment, respectively. The third panel illustrates differential interactions comparing vehicle with GW4064 HiChIP signal along the diagonal, in white and blue colors, corresponding to decreased interactions in vehicle-treated livers. The fourth panel shows differential interactions comparing GW4064 with vehicle HiChIP signal along the diagonal, in dark purple color, corresponding to increased interactions in GW4064. (E) Virtual 4C plot comparing chromatin interactions from a single genomic location (chr11: 1768000) with the rest of the genomic region (chr11: 17600000–17800000), corresponding to the region in black rectangle in the right-most panel in D.

Foxa2 ChIP-Seq (7306 vehicle, 22,666 GW4064)¹³ and found that they are also occupied by Foxa2 in HiChIP data, as expected (Figure 6A). Scanning motif analysis of positional weight matrices in the JASPAR and TRANSFAC databases in Foxa2 binding sites identified a highly enriched forkhead motif bound by Fox transcription factors in both conditions (P value ~ 0), as expected for Foxa2 ChIP. We used these regions to identify Foxa2-anchored intrachromosomal loops (3119 for vehicle, 18,503 for GW4064; Figure 6B). Although 70% of sites bound by Foxa2 in vehicle-treated livers overlapped with regions occupied in livers activated by GW4064,¹³ only about a third of intrachromosomal loops were common to both conditions. A representative region showing more Foxa2-anchored

intrachromosomal loops with agonist treatment is shown in Figure 6C.

We have demonstrated that contrary to the established paradigm, FXR binding changes drastically with addition of an agonist and ligand-dependent FXR binding is Foxa2-dependent.¹³ We proceeded to ascertain whether Foxa2-anchored intrachromosomal loops differed at FXR ligand-independent and ligand-dependent sites. FXR binding is ligand-independent at *Nr0b2* locus¹³ and FXR target *Slc51b* is expressed in the intestine but not in the liver. There are no substantial changes in loops at *Nr0b2* locus and we observe no Foxa2-anchored loops present at *Slc51b* locus (Figure 6D). In contrast, the number of Foxa2-anchored loops drastically increases at several FXR targets with ligand-dependent FXR

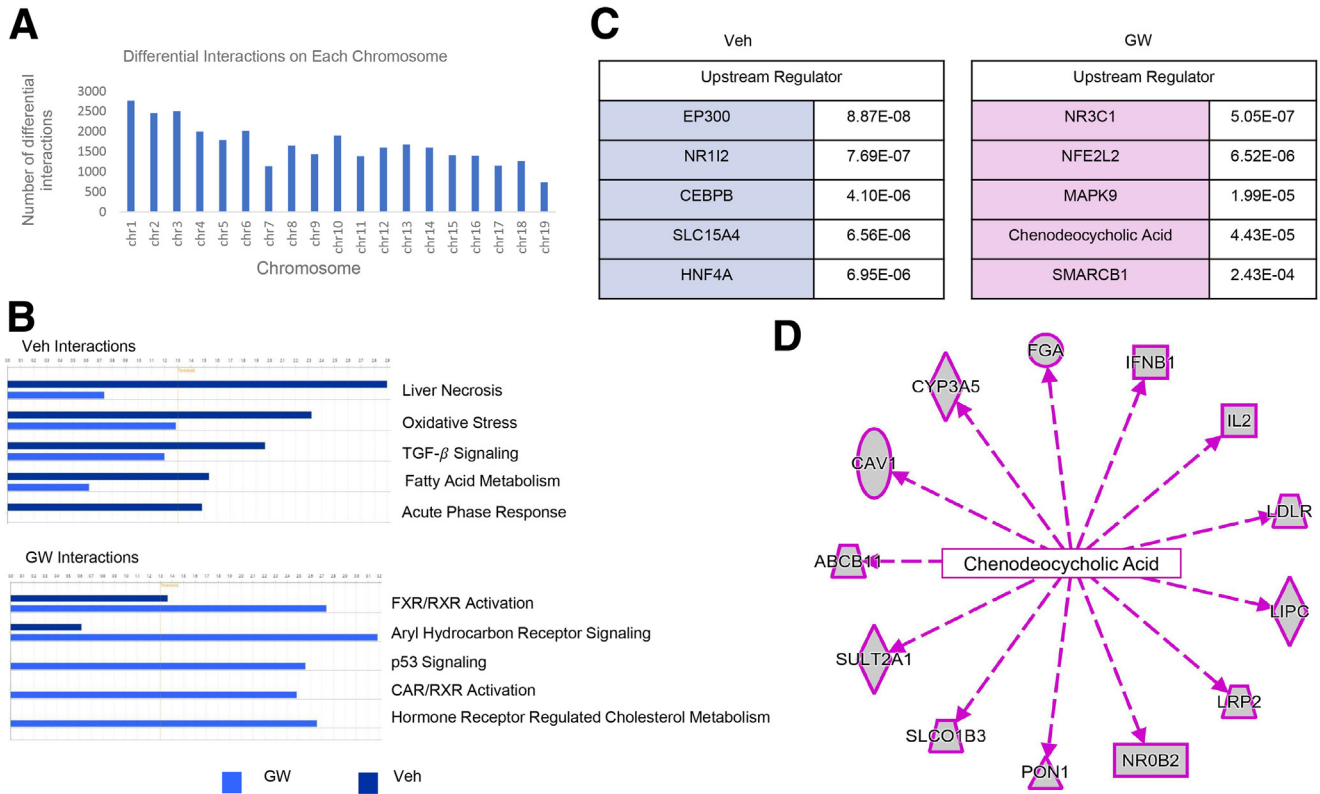


Figure 3. Functional analysis of genome-wide differential interactions. (A) A plot showing the number of differential interactions on each chromosome. (B) Pathways identified by IPA of genes in differential interactions regions include “Oxidative Stress,” “Fatty Acid Metabolism,” and “Acute Phase Response” in control livers, whereas genes in FXR and CAR activation pathways and those regulating cholesterol metabolism were found in agonist-treated livers, consistent with bile acid activation. (C) IPA of genes in differential interaction regions identified multiple upstream regulators, including HNF4 α , CEBPB, and EP300 for control livers and NFE2L2, SMARCB1, and chenodeoxycholic acid. (D) Chenodeoxycholic acid-regulated network identified by IPA for GW-treated livers. Chenodeoxycholic acid is a naturally occurring bile acid that activates FXR. Hence, IPA analysis confirms FXR activation in agonist-treated livers.

binding, including its own locus¹³ (*Nr1i2/PXR*, *Abcb11/Bsep*, *Cyp3a11*, *Nr1h4/FXR*; Figure 6E).

Next, we identified Foxa2-anchored interchromosomal loops (1581 for vehicle, 8463 for GW4064; Figure 7A) and they were mostly distinct for the 2 conditions (overlap 84 loops). Visualization of interchromosomal loops on chromosome 11 (vehicle, left; GW4064, middle; both, right) demonstrates a substantial increase in these interactions with addition of FXR agonist (Figure 7B). We have reported that liver-specific Foxa2 mutants accumulate hepatic bile acids because of decreased transcription of genes encoding bile acid transporters and bile acid conjugation enzymes (*Abcc2*, *Abcc3*, *Abcc4*, *Slco1a4*, *Slc27a5*).^{1,13} We observe novel Foxa2-anchored interchromosomal loops forming in GW-treated livers for these targets responsible for cholestatic phenotype in Foxa2-deficient livers (Figure 7C).

Foxa2 and FXR Ligand-Dependent Binding Correlate with Increase in Intrachromosomal Loops Anchored by Foxa2 and Activation of FXR Targets

To ascertain whether chromatin conformation changes observed with GW treatment had functional consequences,

we integrated interaction data with Foxa2 and FXR binding (Foxa2 ChIP-Seq, FXR ChIP-Seq) and differential gene expression in agonist-treated livers (RNA-Seq) for FXR targets with ligand-dependent binding. We observe that increase in Foxa2-anchored intrachromosomal loops correlates with increased binding of both Foxa2 and FXR and activation of FXR-dependent gene transcription at these loci (*Abcb11/Bsep*, *Cyp3a11*, *Nr1h4/FXR*, *Nr1i2/PXR*; Figure 8).

In summary, we demonstrate that genome-wide chromatin interactions are significantly expanded with ligand activation of FXR. Distribution of TADs changes and the number of Foxa2-anchored loops greatly increase with agonist treatment, leading to distal interactions and activation of FXR-dependent gene expression (Figure 9). Hence, we have identified a novel role for Foxa2 in chromatin conformation dynamics and extended its function in bile acid metabolism.

Discussion

Many transcription factors that orchestrate liver metabolism, including Foxa2¹ and nuclear receptors,² bind distally to the transcription start site of genes.^{3,4} How the

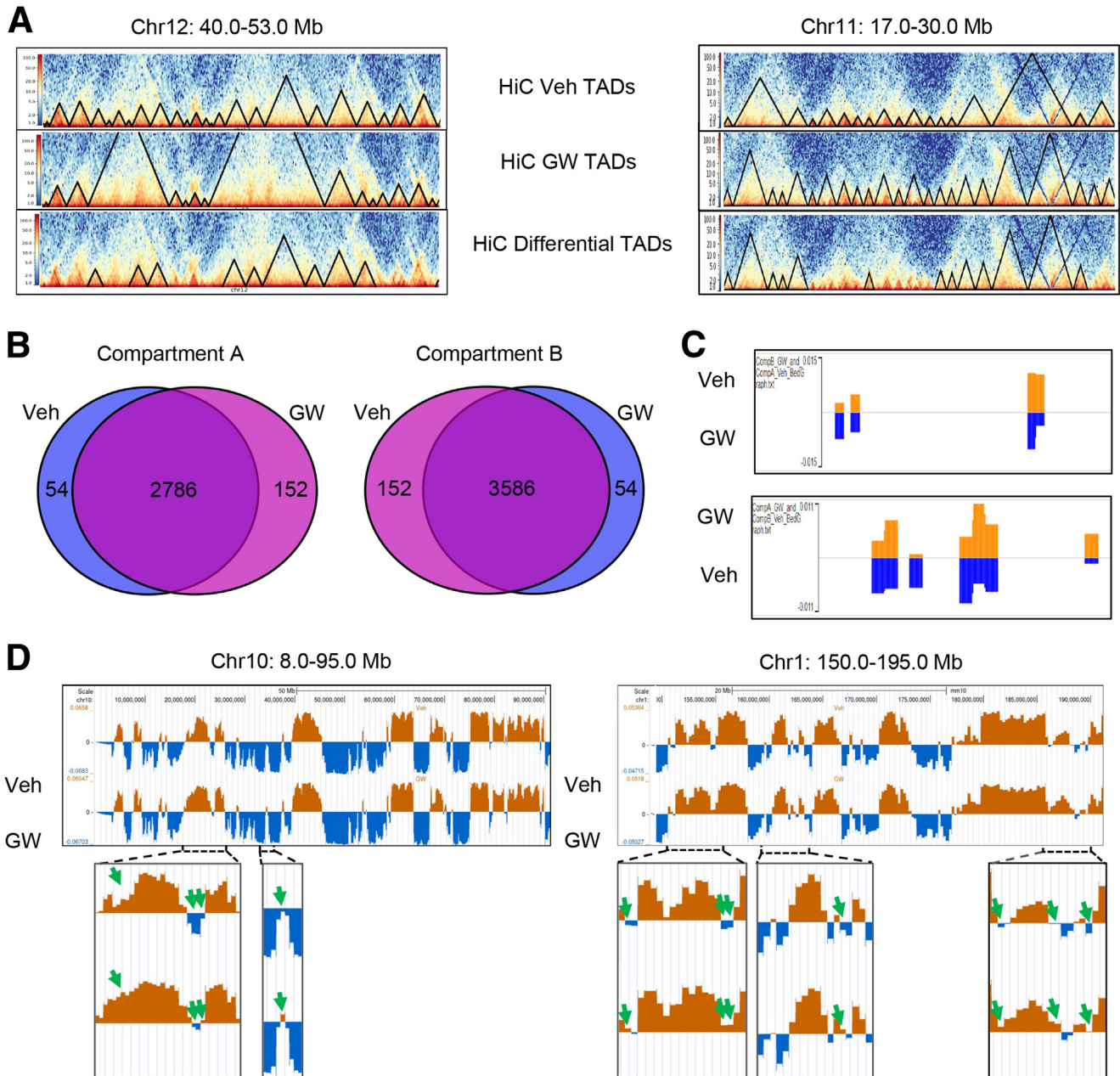


Figure 4. TADs and A/B compartments are reshuffled with the addition of FXR ligands. (A) Comparison of TAD distributions in vehicle and GW4064 for chromatin regions chr12: 40–53.0 Mb (*left*) and chr11: 8.0–20.0 Mb (*right*). TADs in vehicle control (*top*), TADs with agonist treatment (*middle*), differential TADs (*bottom*). The *black triangles* in each panel indicate the separated TAD domains in each condition. (B) Venn diagram comparing activated and repressed regions (Compartment A and Compartment B, respectively) in HiChIP interactions showing that 54 such regions changed from being activated in vehicle-treated to repressed in GW-treated livers, whereas 152 moved from Compartment A in agonist-treated to Compartment B in control livers. (C) Examples of compartment switching (Compartment A in vehicle control to Compartment B in GW4064 treatment, *top*; Compartment B in vehicle control to Compartment A in GW4064 treatment, *bottom*). *Orange* indicates compartment A (active), whereas *blue* indicates compartment B (inactive). (D) Representative comparison of A/B compartments in vehicle control and GW4064-treated livers (chr10: 8.0–95.0 Mb, *left*; chr1: 150.0–195.0 Mb, *right*). *Orange* indicates compartment A (active), whereas *blue* indicates compartment B (inactive). The *green arrows* point at regions switching from inactive in vehicle control to more active in GW4064-treated livers.

distal regulatory elements bound by these factors regulate hepatic gene expression has been largely unexplained. However, liver-specific deletion of CTCF, a protein that

organizes 3-dimensional structure of the genome, leads to steatosis through the effects on nuclear receptor peroxisome proliferator-activated receptor- γ .⁵ In addition, CTCF

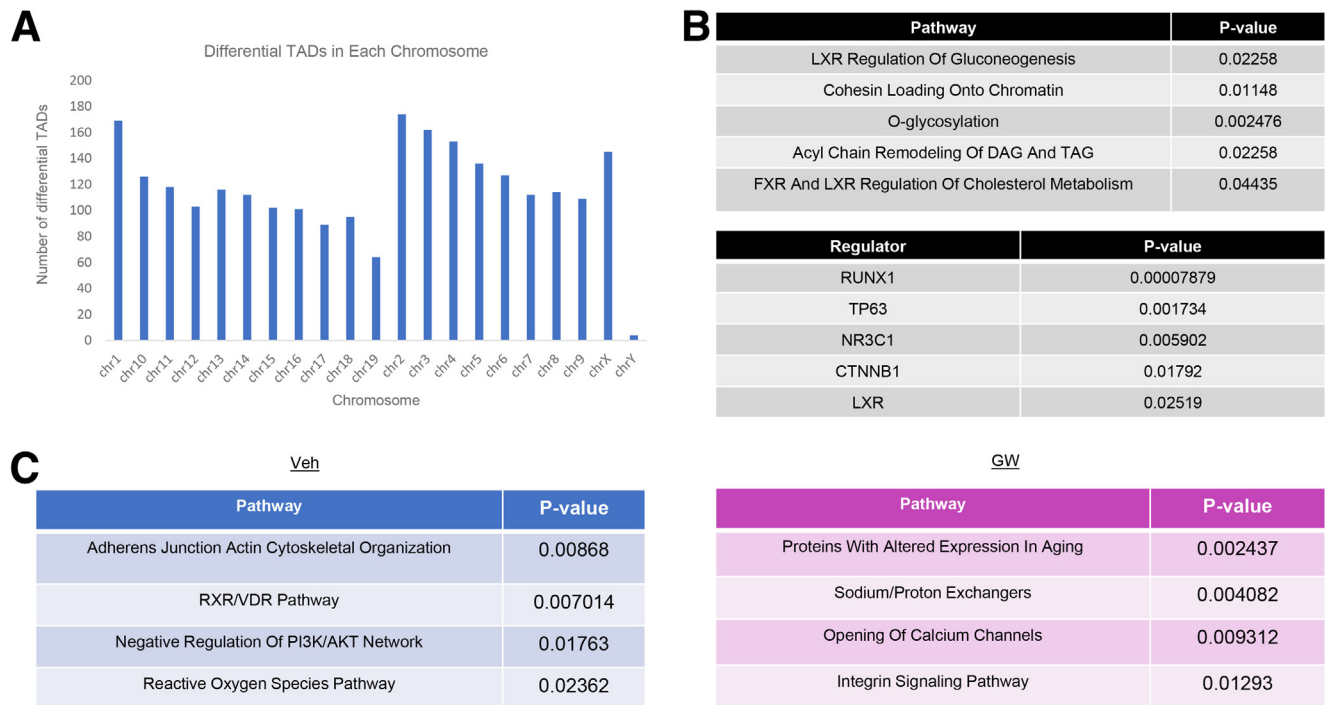


Figure 5. Functional analysis of TADs. (A) A plot showing the number of differential TADs on each chromosome. (B) Enrichr pathway analysis of genes in differential TAD regions identified overrepresented pathways including “LXR regulation of gluconeogenesis” and “FXR and LXR regulation of cholesterol metabolism,” consistent with bile acid activation, and “Cohesin loading onto chromatin,” congruous with cohesin function in mediating chromatin loop formation (*top*). EnrichR ChEA analysis of genes in differential TADs identified overlap with RUNX1, TP53, β -catenin, and LXR targets (*bottom*). (C) Functional analysis of genes in switching compartments shows “Cytoskeletal Organization,” “Reactive Oxygen Species,” and “RXR/VDR pathway” pathways overrepresented in 54 regions repressed with agonist treatment and “Proteins with Altered Expression in Aging,” “Sodium/Proton Exchangers,” and “Opening of Calcium Channels” in 152 regions activated with GW treatment.

and cohesin coordinate chromatin structure for sexually dimorphic gene expression in the liver.⁶

In this study, we demonstrate that the transformation of chromatin landscape with addition of FXR ligand is extensive, far more than expected. We observe a substantial increase in genome-wide interactions, reshuffling of TADs, and compartment switching in GW-treated livers. In addition, the number of both intrachromosomal and interchromosomal Foxa2-anchored loops dramatically changes with ligand addition. Our observations suggest that in addition to opening of chromatin for additional binding, there is a need for substantial chromatin restructuring and additional genome-wide interactions to achieve ligand-dependent activation of gene expression. These findings need to be taken into consideration in development of drug targets to treat medical conditions, such as metabolic disease and cancer.

We have identified several regulators of genes in differential interactions and TAD regions, including NRF2 (*Nfe2l2*), glucocorticoid receptor (GR, NR3C1), Runx1, and β -catenin. Most factors are protective in cholestasis^{22,24,25} (β -catenin, NRF2, Runx1), whereas glucocorticoids promote the disease.²⁶ However, activation of gene expression by these regulators has implications for other disorders, primarily metabolic dysfunction-associated steatotic liver disease (formerly nonalcoholic fatty liver disease) and hepatocellular carcinoma. Dysregulation of NRF2 and

β -catenin are associated with progression of hepatocellular carcinoma,^{27,28} whereas glucocorticoids, Runx1, and β -catenin play a role in pathogenesis of metabolic dysfunction-associated steatotic liver disease.^{29–31}

We have previously challenged the accepted ligand-independent binding mechanism, showing that FXR and LXR α bind to both ligand-independent and ligand-dependent sites in the liver, inaccessible without the ligand, and Foxa2 modulates changes in chromatin accessibility for additional binding during ligand activation.¹³ In this study, we extend our findings, demonstrating drastic alterations in chromatin conformation accompany changes in chromatin accessibility with addition of agonist in ligand-dependent activation of FXR. These results also contest previously accepted mechanism of ligand-dependent activation involving ligand-independent binding. Because we demonstrated that ligand-dependent activation of both FXR and LXR α requires opening of chromatin in a common mechanism, we anticipate that chromatin conformation changes observed with addition of FXR agonist will also be shared in ligand-dependent activation of LXR α and likely for other type II nuclear receptors.

We have described an extensive role for Foxa2 in hepatic bile acid metabolism^{1,13,14} and synergistic cooperation between Foxa2 and bile acid receptor FXR in activating ligand-dependent gene expression.^{13,14} Here we demonstrate that Foxa2 also mediates chromatin conformation changes that

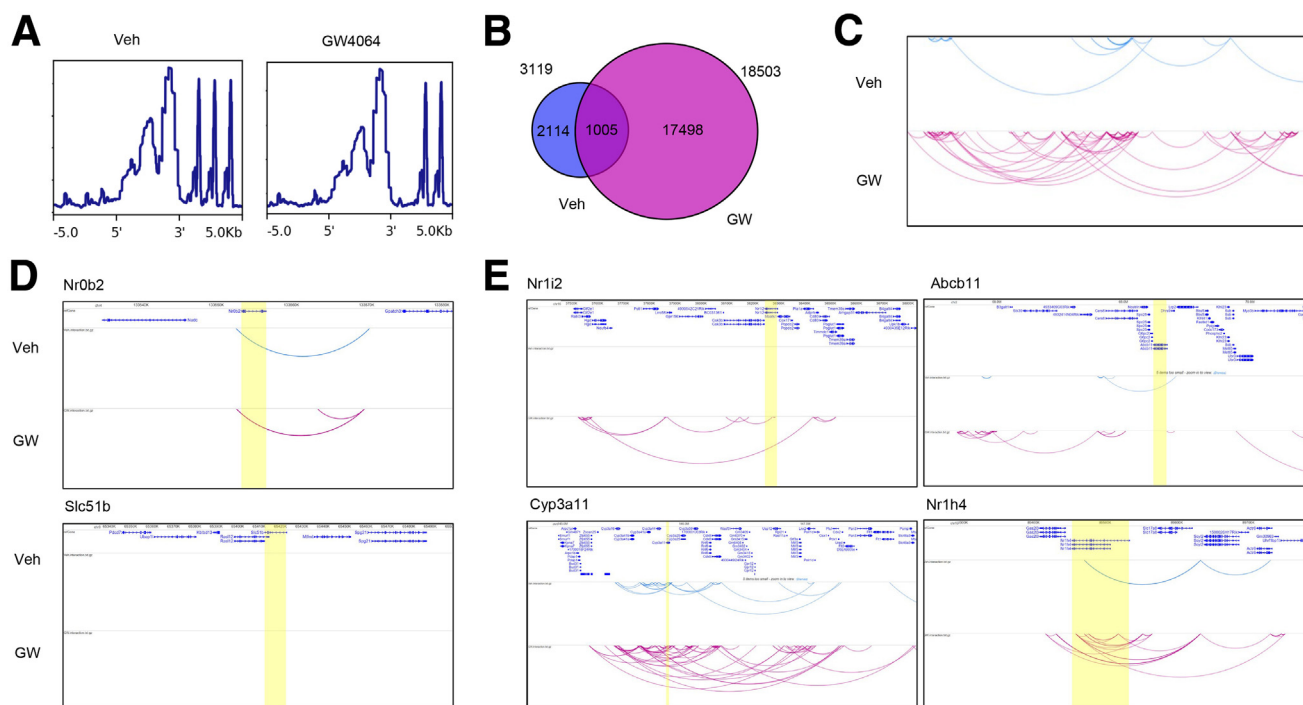


Figure 6. Foxa2-anchored intrachromosomal loops are drastically increased during ligand-dependent activation of FXR. (A) Foxa2 HiChIP signal (RPKM) plot at Foxa2 binding sites from Foxa2 ChIP-Seq (7306 sites vehicle, 22666 GW4064).¹³ (B) Venn diagram comparing Foxa2-anchored intrachromosomal loops in vehicle and GW4064-treated livers. There are totally 3119 intraloops unique to vehicle control, 18,503 intraloops unique to GW4064 treatment, and 1005 intraloops common to both conditions. (C) Representative arc plot showing total Foxa2-anchored intrachromosomal loops within the genomic region chr10: 66.7–69.8 Mb in vehicle and GW4064 treatment. (D) Representative arc plots showing intrachromosomal loops at FXR targets with ligand-independent binding (*Nr0b2* and *Slc51b*). (E) Representative arc plots showing the number of Foxa2-anchored intrachromosomal loops drastically increases at a number of FXR targets with ligand-dependent FXR binding, including its own locus (*Nr1i2*/PXR, *Abcb11*/Bsep, *Cyp3a11*, *Nr1h4*/FXR).

accompany activation of FXR. Specifically, we observe drastic increase in Foxa2-anchored intrachromosomal loops at FXR locus and loci of FXR targets *Abcb11*/Bsep, *Cyp3a11*, and *Nr1i2*/PXR and novel Foxa2-anchored interchromosomal loops at Foxa2 targets that are responsible for cholestatic phenotype. Hence, Foxa2 plays a new role in enabling these structural changes, extending its function in bile acid homeostasis.

Methods

Animals

Wild-type male mice, 8–12 weeks of age, were used for all studies. Ligand activation was performed as described previously.¹³ Briefly, mice were treated once with FXR agonist GW4064 via oral gavage. Control mice were treated with vehicle (20 mL propylene glycol/5 mL Tween 80 solution). Animals on control and experimental treatments were sacrificed 4 hours after gavage. All animal work was approved by Animal Care and Use Committee at the University of Virginia (protocol number 4162-03-20).

HiChIP Assay

HiChIP experiments were performed with vehicle- and ligand-treated mouse liver tissues using the Arima-HiC+ Kit according to manufacturer's protocol.

Pulverization and Crosslinking of Liver Tissues. About 200 mg of each mouse liver tissue was pulverized using Covaris CryoPrep System with impact level setting 3. Pulverized tissues were washed with cold 1xPBS and pelleted by centrifugation at $1000 \times g$ at 4°C for 5 minutes. Three milliliters of TLB1 was added to resuspend each sample. After incubation for 20 minutes at 4°C , samples were filtered through 40- μm cell strainers. The flowthrough was pelleted by centrifugation at $1000 \times g$ at 4°C for 5 minutes and resuspended in 1 mL of TLB2. Then, 3 mL of Sucrose Solution was carefully overlaid on top of the samples and pelleted by centrifugation at 4°C for 5 minutes. Samples were then resuspended in 5 mL 1xPBS and crosslinked by adding 286 μL of 37% formaldehyde to achieve a final concentration of 2% (wt/vol) and incubated at room temperature for 10 minutes. Then, 460 μL of Stop Solution 1 was added, samples were incubated at room temperature for 5 minutes, and then on ice for 15 minutes. Samples were pelleted by centrifugation at $2500 \times g$ at 4°C for 5 minutes and resuspended in 1 mL cold 1xPBS. An aliquot that contains the equivalent of 10 mg of original pulverized tissue for each sample was then measured by Qubit 4 Fluorometer for total DNA yield.

HiChIP Preparation. The crosslinked samples that contained the equivalent of 15 μg of total DNA for each sample

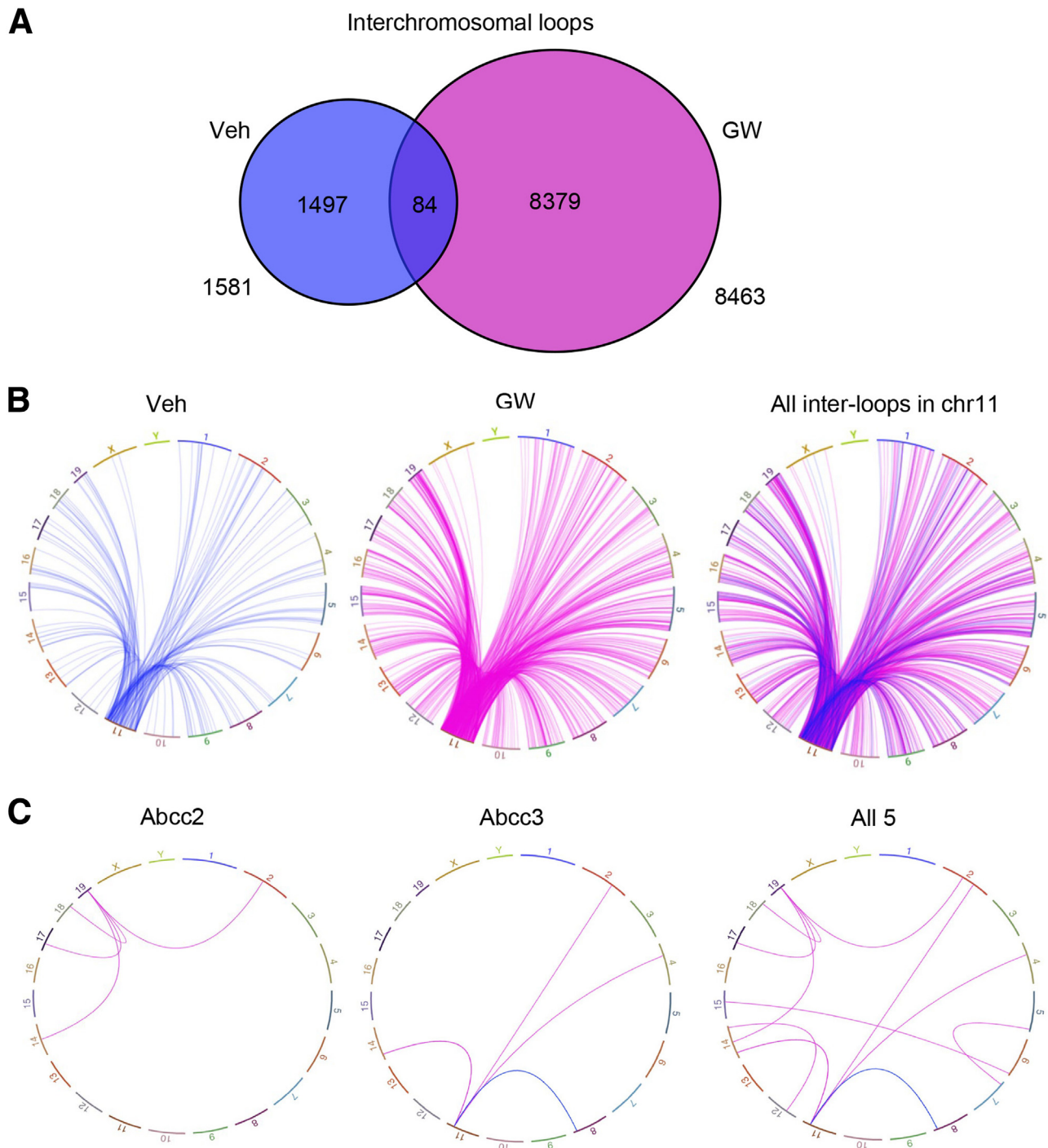


Figure 7. Foxa2-anchored interchromosomal loops are significantly increased in the presence of FXR ligand for activation. (A) Venn diagram comparing Foxa2-anchored interchromosomal loops in vehicle and GW4064-treated livers (1581 for vehicle, 8463 for GW4064, 84 common) shows they were mostly distinct for the 2 conditions. (B) Visualization (IGV circle view) of interchromosomal loops on chromosome 11 (vehicle, *left*; GW4064, *middle*; both, *right*) demonstrates a substantial increase in these interactions with addition of FXR agonist. (C) Novel Foxa2-anchored interchromosomal loops form in GW-treated livers at Foxa2 targets responsible for cholestatic phenotype in Foxa2-deficient livers.¹

were resuspended in 20 μL of lysis buffer and incubated at 4°C for 20 minutes. Then, 24 μL of Conditioning Solution was added and samples were incubated at 62°C for 10 minutes. Then, 20 μL of Stop Solution 2 was added and

samples were placed at 37°C for 15 minutes. A master mix of 7 μL of buffer A, 1 μL of enzyme1 μL of restriction enzyme MboI, and 1 μL of restriction enzyme of HinfI were added to each sample, and samples were incubated at 37°C for

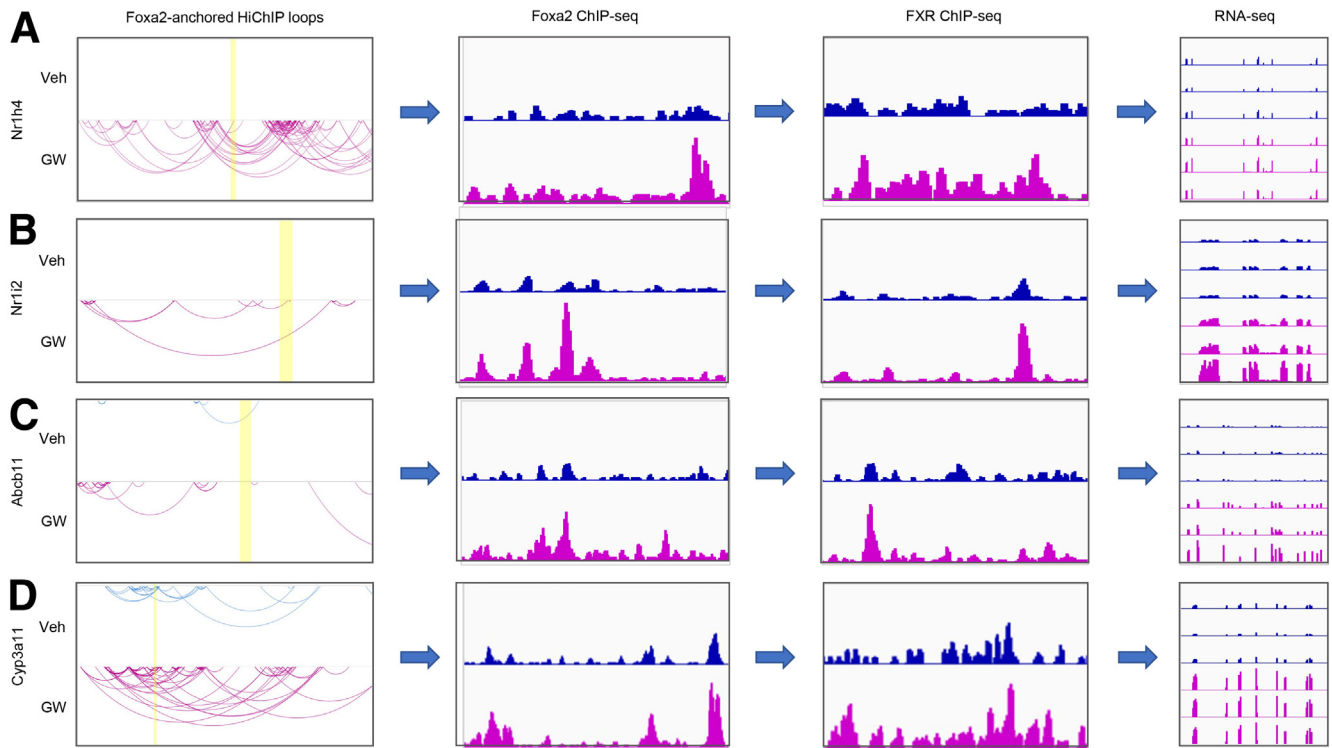


Figure 8. Foxxa2 and FXR ligand-dependent binding correlate with increase in intrachromosomal loops anchored by Foxxa2 and activation of FXR targets. Increase in Foxxa2-anchored intrachromosomal loops correlates with increased binding of Foxxa2 and FXR and activation of FXR-dependent gene transcription at loci with FXR ligand-dependent binding (A) *Abcb11*/*Bsep*, (B) *Cyp3a11*, (C) *Nr1h4*/FXR, and (D) *Nr1i2*/PXR.

1 hour. Samples were then pelleted at $2500 \times g$ at 4°C for 5 minutes. Next, samples were gently rinsed in 1.5 mL of dH_2O , pelleted, and resuspended in $75 \mu\text{L}$ of dH_2O . Then, $16 \mu\text{L}$ of master mix containing $12 \mu\text{L}$ of Buffer B and $4 \mu\text{L}$ of Enzyme B was added to each sample, mixed well, and incubated at room temperature for 45 minutes. Next, $82 \mu\text{L}$ master mix containing $70 \mu\text{L}$ of Buffer C and $12 \mu\text{L}$ of Enzyme C was added to each sample, mixed well, and incubated at room temperature for 15 minutes. Samples were then pelleted and resuspended in $110 \mu\text{L}$ of cold R1 Buffer (10 mM Tris-HCl pH8.0, 140 mM NaCl, 1 mM EDTA, 1% Triton X-100, 0.1% sodium dodecyl sulfate, 0.1% sodium deoxycholate) and incubated at 4°C for 20 minutes. Chromatin shearing was then performed using Diagenode Bioruptor Pico with “30sec ON/30sec OFF” condition for 11–12 cycles. Then, $900 \mu\text{L}$ of R1 Buffer was added to each sheared sample to get total volume of 1 mL. For Foxxa2 HiChIP immunoprecipitation, $3.5 \mu\text{L}$ of Foxxa2 antibody (Seven Hills Bioreagents WRAB-1200) was added to each sample and incubated at 4°C overnight with rotating. Next day, $30 \mu\text{L}$ of preblocked Protein G beads was added to each sample and incubated at 4°C for 4 hours with rotating. After incubation, beads were sequentially washed 3 times with R1 Buffer, 2 times with R3 Buffer (0.1% sodium dodecyl sulfate, 1% Triton X-100, 2 mM EDTA, 20 mM Tris-HCl pH 8.5, 0.1% sodium deoxycholate and 300 mM NaCl), 1 time with LC Buffer (1 mM EDTA, 10 mM Tris-HCl pH 8.5, 0.1% sodium deoxycholate and 150 mM lithium chloride, 0.5% IGEPAL

CO-630), and 2 times with LTE Buffer (10 mM Tris-HCl pH 8.0, and 0.1 mM EDTA). The beads of each sample were resuspended with $174 \mu\text{L}$ of Elution Buffer. Then, $35.5 \mu\text{L}$ of master mix containing $10.5 \mu\text{L}$ of Buffer D and $25 \mu\text{L}$ of Enzyme D and $20 \mu\text{L}$ of Buffer E was added to each sample, and incubated at 55°C for 30 minutes, 68°C for 90 minutes, and 25°C for 10 minutes. The bead-bound DNA for each sample was purified with $230 \mu\text{L}$ of AMPure XP beads and washed 2 times with $700 \mu\text{L}$ of 80% ethanol, then resuspended thoroughly in $50 \mu\text{L}$ of Elution Buffer. DNA concentrations were measured using Qubit 1x dsDNA HS Assay Kit.

Biotin Enrichment and HiChIP Library Preparation. Elution Buffer was added to beads-bound DNA to bring the total volume to $100 \mu\text{L}$ for each sample. Then, $100 \mu\text{L}$ of Enrichment Beads were added, mixed well, and incubated at RT for 15 minutes. Beads were washed 2 times with $200 \mu\text{L}$ of Wash Buffer and 1 time with $100 \mu\text{L}$ of Elution Buffer, then resuspended in $40 \mu\text{L}$ of Elution Buffer.

For end-repair and adaptor ligation, $20 \mu\text{L}$ of a master mix containing $13 \mu\text{L}$ of Low EDTA TE, $6 \mu\text{L}$ of Buffer W1, and $1 \mu\text{L}$ of Enzyme W2 was added to each sample, and incubated at 37°C for 10 minutes. Beads were washed twice with $150 \mu\text{L}$ of Wash Buffer and once with $100 \mu\text{L}$ of Elution Buffer, then resuspended in $50 \mu\text{L}$ of a master mix containing $30 \mu\text{L}$ of Low EDTA TE, $5 \mu\text{L}$ of Buffer G1, $13 \mu\text{L}$ of Reagent G2, $1 \mu\text{L}$ of Enzyme G3, and $1 \mu\text{L}$ Enzyme G4, and incubated at 20°C for 20 minutes. Beads were washed twice

Bile Acid/FXR target

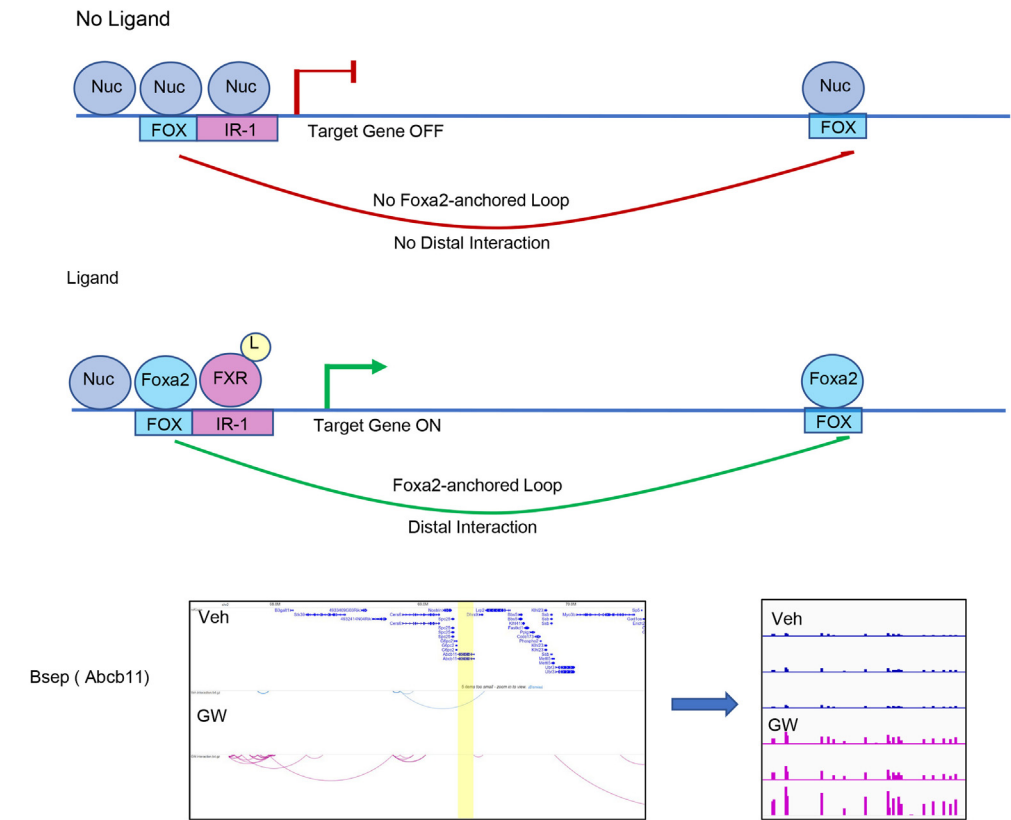


Figure 9.A a model describing how Foxa2 mediates chromatin conformation changes in ligand-dependent activation of FXR. We have shown that Foxa2 binding is increased when FXR is activated with its ligand GW4064.¹³ Additional Foxa2 binding in ligand-activated state leads to formation of Foxa2-anchored loops (*middle*), leading to distal interactions and activation of gene expression of targets in bile acid metabolism, such as Bsep (Abcb11, *bottom*).

with 150 μ L of Wash Buffer and once with 100 μ L of Elution Buffer. Then, beads were resuspended in 25 μ L of a master mix containing 20 μ L of Low EDTA TE, 3 μ L of Buffer Y, 2 μ L of Enzyme Y3 and 5 μ L of uniquely indexed Reagent Y2, mixed well, and incubated at 25°C for 15 minutes. Beads were washed twice with 150 μ L of Wash Buffer and once with 100 μ L of Elution Buffer. Then, resuspended in 50 μ L of a master mix containing 30 μ L of Low EDTA TE, 5 μ L of Buffer B1, 2 μ L of Reagent B2, 9 μ L of Reagent B3, 1 μ L of Enzyme B4, 2 μ L of Enzyme B5, and 1 μ L of Enzyme B6, mixed well, and incubated at 40°C for 10 minutes. Beads were washed twice with 150 μ L of Wash Buffer and 1 time with 100 μ L of Elution Buffer. Then, resuspended in 22 μ L of Elution Buffer. These HiChIP libraries were then amplified using Accel-NGS 2S Plus DNA Library Kit for Illumina Platforms and Accel-NGS 2S Indexing Kit (Set A) for Illumina Platforms (Swift Biosciences, Cat# 26148).

Illumina Sequencing. The HiChIP libraries were deep sequenced using the Illumina NextSeq 2000 Sequencer in paired-end 2 \times 150 bp mode using the NextSeq 1000/2000 P2 Reagents (300 Cycles) sequencing kit.

HiChIP Data Analysis

HiChIP Data Processing with HiC-Pro. HiChIP paired-end reads were aligned to mm10 genome assembly using the HiC-Pro pipeline¹⁶ using bowtie2 (version 2.2.9) and

with mapping quality filter 15. Default settings were used to remove singleton, multimapped, and duplicate reads. Reads were assigned to MboI (-GATC) and HinfI (G-ANTC) restriction fragments and filtered for valid interactions using minimum and maximum size parameters of 100 and 100,000, and binned interaction matrices were generated. **HiChIP Significant Contact Calling with HiCCUPS and Fit-Hi-C.** HiCCUPS³² did not run on the interaction matrix because of sparsity. Instead, we used Fit-Hi-C contact caller.³³ Bin pairs of the interaction matrix with statistically significant contact signals were identified using Fit-Hi-C. Genome-wide intrachromosomal bin pairs were filtered for an interaction distance between 20 kb and 2 Mb, and default Fit-HiC settings were used to calculate FDR values for each bin pair in a given HiChIP experiment. Bin size of 50 kb and FDR cutoff <0.001 were used to identify significant contacts.

HiChIP Differential Significant Contact Calling with HiCcompare. HiCcompare³⁴ uses the raw Hi-C matrix of HiC-Pro output as input. Two Hi-C matrices were jointly normalized for each chromosome. The default settings were used. The interactions with low average expression were filtered out with A.min = 15. The value of FDR <0.05 was used for differential contact selection.

TAD Calling with HiCExplorer. TADs were called with HiCExplorer.³⁵ Hi-C contact matrix was used as input. TAD-separation scores were calculated for all bins. The

TAD-separation scores were evaluated and the cutoff P values $< .05$ were applied to select the TAD boundaries.

Compartment A/B Profile Calling with cworld. Compartments were called using cworld.³⁶

Genomic bins of reference genome were generated at 250 kb. The command matrix2compartment command was used to extract the compartment A/B profiles with default settings. *Foxa2-Anchored Loops Calling with hichipper.* The hichipper (version 0.7.7)³⁷ was used to identify the Foxa2-anchored chromatin loops. The HiC-Pro matrix output, restriction digested mm10 genome assembly, and ChIP-Seq Foxa2 binding sites¹³ were used as input to identify chromatin loops extending from regions occupied by Foxa2. The default parameter settings were used with minimum distance of 5000 and maximum peak padding width of 2,000,000.

Visualization of HiChIP Matrices, Loops, and Compartment A/B Profiles. Hi-C matrices were visualized using Juicebox.¹⁸ Foxa2-anchored intrachromosomal and interchromosomal loops were visualized using WashU Epigenome Browser,³⁸ Integrative Genome Viewer,¹⁹ and UCSC Genome Browser. Compartment A/B profiles were visualized using UCSC Genome Browser.³⁹

Functional Analysis. Interaction regions were associated with closest genes using GREAT,¹⁷ which were subsequently used for pathway analysis with Enrichr²⁰ and IPA as described previously.^{13,40} Scanning motif analysis for over-represented transcription factor binding motifs in interaction regions was performed by PscanChIP.⁴¹ Plots of HiChIP coverage were generated by deepTools.⁴² The overlap between different categories of interactions was computed using bedtools (version 2.29.2).⁴³

References

- Bochkis IM, Rubins NE, White P, et al. Hepatocyte-specific ablation of Foxa2 alters bile acid homeostasis and results in endoplasmic reticulum stress. *Nat Med* 2008;14:828–836.
- Rudraiah S, Zhang X, Wang L. Nuclear receptors as therapeutic targets in liver disease: are we there yet? *Annu Rev Pharmacol Toxicol* 2016;56:605–626.
- Bochkis IM, Schug J, Ye DZ, et al. Genome-wide location analysis reveals distinct transcriptional circuitry by paralogous regulators Foxa1 and Foxa2. *PLoS Genet* 2012;8:e1002770.
- Biddie SC, John S, Hager GL. Genome-wide mechanisms of nuclear receptor action. *Trends Endocrinol Metab* 2010;21:3–9.
- Choi Y, Song MJ, Jung WJ, et al. Liver-specific deletion of mouse CTCF leads to hepatic steatosis via augmented PPAR γ signaling. *Cell Mol Gastroenterol Hepatol* 2021;12:1761–1787.
- Matthews BJ, Waxman DJ. Impact of 3D genome organization, guided by cohesin and CTCF looping, on sex-biased chromatin interactions and gene expression in mouse liver. *Epigenetics Chromatin* 2020;13:30.
- Dehingia B, Milewska M, Janowski M, et al. CTCF shapes chromatin structure and gene expression in health and disease. *EMBO Rep* 2022;23:e55146.
- Lin CY, Gustafsson JA. Targeting liver X receptors in cancer therapeutics. *Nat Rev Cancer* 2015;15:216–224.
- Wright MB, Bortolini M, Tadayyon M, et al. Minireview: challenges and opportunities in development of PPAR agonists. *Mol Endocrinol* 2014;28:1756–1768.
- Schaap FG, Trauner M, Jansen PL. Bile acid receptors as targets for drug development. *Nat Rev Gastroenterol Hepatol* 2014;11:55–67.
- Ma Z, Deng C, Hu W, et al. Liver X receptors and their agonists: targeting for cholesterol homeostasis and cardiovascular diseases. *Curr Issues Mol Biol* 2017;22:41–64.
- Kidani Y, Bensinger SJ. Liver X receptor and peroxisome proliferator-activated receptor as integrators of lipid homeostasis and immunity. *Immunol Rev* 2012;249:72–83.
- Kain J, Wei X, Reddy NA, et al. Pioneer factor Foxa2 enables ligand-dependent activation of type II nuclear receptors FXR and LXR α . *Mol Metab* 2021;53:101291.
- Bochkis IM, Schug J, Rubins NE, et al. Foxa2-dependent hepatic gene regulatory networks depend on physiological state. *Physiol Genomics* 2009;38:186–195.
- Bochkis IM, Shin S, Kaestner KH. Bile acid-induced inflammatory signaling in mice lacking Foxa2 in the liver leads to activation of mTOR and age-onset obesity. *Mol Metab* 2013;2:447–456.
- Servant N, Varoquaux N, Lajoie BR, et al. HiC-Pro: an optimized and flexible pipeline for Hi-C data processing. *Genome Biol* 2015;16:259.
- McLean CY, Bristor D, Hiller M, et al. GREAT improves functional interpretation of cis-regulatory regions. *Nat Biotechnol* 2010;28:495–501.
- Kuleshov MV, Jones MR, Rouillard AD, et al. Juicebox provides a visualization system for Hi-C contact maps with unlimited zoom. *Cell Syst* 2016;3:99–101.
- Robinson JT, Thorvaldsdottir H, Winckler W, et al. Integrative genomics viewer. *Nat Biotechnol* 2011;29:24–26.
- Kuleshov MV, Jones MR, Rouillard AD, et al. Enrichr: a comprehensive gene set enrichment analysis web server 2016 update. *Nucleic Acids Res* 2016;44:W90–97.
- Chien R, Zeng W, Ball AR, et al. Cohesin: a critical chromatin organizer in mammalian gene regulation. *Biochem Cell Biol* 2011;89:445–458.
- Zhang L, Pan Q, Zhang L, et al. Runt-related transcription factor-1 ameliorates bile acid-induced hepatic inflammation in cholestasis through JAK/STAT3 signaling. *Hepatology* 2023;77:1866–1881.
- Kim DH, Lee JW. Tumor suppressor p53 regulates bile acid homeostasis via small heterodimer partner. *Proc Natl Acad Sci U S A* 2011;108:12266–12270.
- Thompson MD, Moghe A, Cornuet P, et al. β -Catenin regulation of farnesoid X receptor signaling and bile acid metabolism during murine cholestasis. *Hepatology* 2018; 67:955–971.
- Okada K, Shoda J, Taguchi K, et al. Nrf2 counteracts cholestatic liver injury via stimulation of hepatic defense systems. *Biochem Biophys Res Commun* 2009; 389:431–436.
- Lu Y, Zhang Z, Xiong X, et al. Glucocorticoids promote hepatic cholestasis in mice by inhibiting the transcriptional activity of the farnesoid X receptor. *Gastroenterology* 2012;143:1630–1640.

27. Raghunath A, Sundarraj K, Arfuso F, et al. Dysregulation of Nrf2 in hepatocellular carcinoma: role in cancer progression and chemoresistance. *Cancers (Basel)* 2018; 10:481.
28. Xu C, Xu Z, Zhang Y, et al. β -Catenin signaling in hepatocellular carcinoma. *J Clin Invest* 2022;132:e154515.
29. Rahimi L, Rajpal A, Ismail-Beigi F. Glucocorticoid-induced fatty liver disease. *Diabetes Metab Syndr Obes* 2020;13:1133–1145.
30. Kaur S, Rawal P, Siddiqui H, et al. Increased expression of RUNX1 in liver correlates with NASH activity score in patients with non-alcoholic steatohepatitis (NASH). *Cells* 2019;8:1277.
31. Shree Harini K, Ezhilarasan D. Wnt/beta-catenin signaling and its modulators in nonalcoholic fatty liver diseases. *Hepatobiliary Pancreat Dis Int* 2023; 22:333–345.
32. Rao SS, Huntley MH, Durand NC, et al. A 3D map of the human genome at kilobase resolution reveals principles of chromatin looping. *Cell* 2014;159:1665–1680.
33. Ay F, Bailey TL, Noble WS. Statistical confidence estimation for Hi-C data reveals regulatory chromatin contacts. *Genome Res* 2014;24:999–1011.
34. Stansfield JC, Cresswell KG, Vladimirov VI, et al. HiCcompare: an R-package for joint normalization and comparison of Hi-C datasets. *BMC Bioinformatics* 2018;19:279.
35. Ramírez F, Bhardwaj V, Arrigoni L, et al. High-resolution TADs reveal DNA sequences underlying genome organization in flies. *Nat Commun* 2018;9:189.
36. Sanders JT, Gollosi R, Das P, et al. Loops, topologically associating domains, compartments, and territories are elastic and robust to dramatic nuclear volume swelling. *Sci Rep* 2022;12:4721.
37. Lareau CA, Aryee MJ. hichipper: a preprocessing pipeline for calling DNA loops from HiChIP data. *Nat Methods* 2018;15:155–156.
38. Li D, Purushotham D, Harrison JK, et al. WashU Epi-genome Browser update 2022. *Nucleic Acids Res* 2022; 50:W774–781.
39. Kent WJ, Sugnet CW, Furey TS, et al. The human genome browser at UCSC. *Genome Res* 2002;12:996–1006.
40. Wei X, Murphy MA, Reddy NA, et al. Redistribution of lamina-associated domains reshapes binding of pioneer factor FOXA2 in development of nonalcoholic fatty liver disease. *Genome Res* 2022;32:1981–1992.
41. Zambelli F, Pesole G, Pavesi G. PscanChIP: Finding over-represented transcription factor-binding site motifs and their correlations in sequences from ChIP-Seq experiments. *Nucleic Acids Res* 2013, 41(Web Server issue):W535–543.
42. Ramirez F, Dundar F, Diehl S, et al. deepTools: a flexible platform for exploring deep-sequencing data. *Nucleic Acids Res* 2014, 42(Web Server issue):W187–191.
43. Quinlan AR, Hall IM. BEDTools: a flexible suite of utilities for comparing genomic features. *Bioinformatics* 2010; 26:841–842.

Received September 4, 2023. Accepted October 20, 2023.

Correspondence

Address correspondence to: Irina M. Bochkis, PhD, Department of Pharmacology, University of Virginia School of Medicine, 5026 Pinn Hall, 1340 Jefferson Park Avenue, Charlottesville, Virginia 22908. e-mail: imb3q@virginia.edu.

Acknowledgements

The authors thank Joseph Schinderle, Nihal Reddy, and Benjamin Weidemann for technical assistance. Lu Han and Anqi Wu contributed equally to this work.

CRedit Authorship Contributions

Yi Hao (Formal analysis: Lead; Investigation: Lead; Software: Equal; Visualization: Equal; Writing – review & editing: Supporting)
 Lu Han (Data curation: Equal; Formal analysis: Equal; Software: Equal; Visualization: Equal; Writing – review & editing: Supporting)
 Anqi Wu (Data curation: Equal; Formal analysis: Equal; Software: Equal; Visualization: Equal; Writing – review & editing: Supporting)
 Irina M. Bochkis, PhD (Conceptualization: Lead; Formal analysis: Supporting; Funding acquisition: Lead; Methodology: Equal; Project administration: Lead; Supervision: Lead; Writing – original draft: Lead)

Conflicts of interest

The authors disclose no conflicts.

Funding

Irina M. Bochkis is supported by National Institute of Diabetes and Digestive and Kidney Diseases R01 award DK121059.